Quantum-Limited Amplification and Entanglement in Coupled Nonlinear Resonators

C. Eichler,[1,*] Y. Salathe,[1] J. Mlynek,[1] S. Schmidt,[2] and A. Wallraff[1]

[1]*Department of Physics, ETH Zürich, CH-8093 Zürich, Switzerland*
[2]*Institute for Theoretical Physics, ETH Zürich, CH-8093 Zürich, Switzerland*

We demonstrate a coupled cavity realization of a Bose-Hubbard dimer to achieve quantum-limited amplification and to generate frequency entangled microwave fields with squeezing parameters well below -12 dB. In contrast to previous implementations of parametric amplifiers, our dimer can be operated both as a degenerate and as a nondegenerate amplifier. The large measured gain-bandwidth product of more than 250 MHz for the nondegenerate operation and the saturation at input photon numbers as high as 2000 per μs are both expected to be improvable even further, while maintaining wide frequency tunability of about 2 GHz. Featuring flexible control over all relevant system parameters, the presented Bose-Hubbard dimer based on lumped element circuits has significant potential as an elementary cell in nonlinear cavity arrays for quantum simulations.

The high level of control achievable over collections of massive or massless particles, such as atoms, spins, or photons, enables the detailed study of intricate many-body phenomena in manmade quantum systems [1]. In this context coupled nonlinear resonators both provide a viable avenue for studying light-matter interactions and constitute a generic building block for photonic quantum simulators of strongly interacting systems [2–4]. Therefore, their theoretical and experimental investigation is pursued in a wide variety of physical settings such as photonic structures [5,6], optomechanical systems [7–9], and superconducting circuits [10–12]. The remarkable progress in quantum science using microwave radiation has stimulated broad interest in low noise amplification [13,14] and has lead to the development of novel versatile amplifiers in recent years [15–23]. Many of these implementations rely on parametric processes in which the noise temperature of the amplifier is solely limited by the radiation temperature of the input fields, ultimately by the vacuum fluctuations [24]. In parametric amplification the presence of a signal stimulates conversion processes from a pump field into the signal field, while creating an additional idler field. When signal and idler fields occupy the same mode, this is referred to as degenerate parametric amplification, whereas in nondegenerate amplifiers the signal and idler modes are separated either spatially or in frequency [24]. While degenerate parametric amplifiers [15] are often preferable for the fast dispersive readout of qubits [25] in quantum feedback protocols [26], nondegenerate amplification [19] can be more practical for multiplexed readout [27], the measurement of photon correlation functions [28], and more general applications in which amplification is to be independent of the phase of the signal relative to the pump. The cavity dimer presented here can be operated in both modes of amplification—degenerate and nondegenerate.

The underlying mechanism is not specific to superconducting circuits and may also be realized using mechanical, optical, or atomic systems.

We consider a system described by two bosonic modes a_L and a_R, which are coupled with hopping rate J and have an on-site interaction strength $U = U_L = U_R$; see generic representation in Fig. 1(a). In a frame rotating at the bare cavity frequency $\omega_0 = \omega_L = \omega_R$ the system is described by the Bose-Hubbard-dimer Hamitonian [29]:

$$H/\hbar = J(a_L a_R^\dagger + a_R a_L^\dagger) + \frac{U}{2}[(a_L^\dagger)^2 a_L^2 + (a_R^\dagger)^2 a_R^2].$$

While the left mode (L) is coupled with rate κ to a transmission line, the right mode (R) is only coupled to the left mode. We consider the parameter regime $|U| \ll J \lesssim \kappa$ to achieve quantum-limited amplification. We note that the design presented below allows us to realize circuits in which any of the three rates may dominate over the other two. Because of the hopping term J the left and right modes hybridize and form symmetric and antisymmetric eigenmodes, a_+ and a_-. The corresponding eigenfrequencies are split by $2J = \omega_+ - \omega_-$ around the bare cavity frequency, ω_0. A coherent drive field $\alpha_{\rm in}$ applied to the dimer in combination with the nonlinearity U shifts the effective resonance frequencies to $\tilde{\omega}_-$ and $\tilde{\omega}_+$; see Fig. 1(b). The effect of finite detuning $\omega_L - \omega_R$ between the left and right mode and unequal interaction strengths $U_L \neq U_R$ are considered in the Supplemental Material [30].

We have calculated the phase diagram of the Bose-Hubbard dimer when driven coherently at a detuning δ from the bare cavity frequency ω_0 using a semiclassical approximation. For drive rates $|\alpha_{\rm in}|^2$ on the order of κ^2/U, the system undergoes a sharp transition from a regime with one stable solution (S) into either a multistable region with
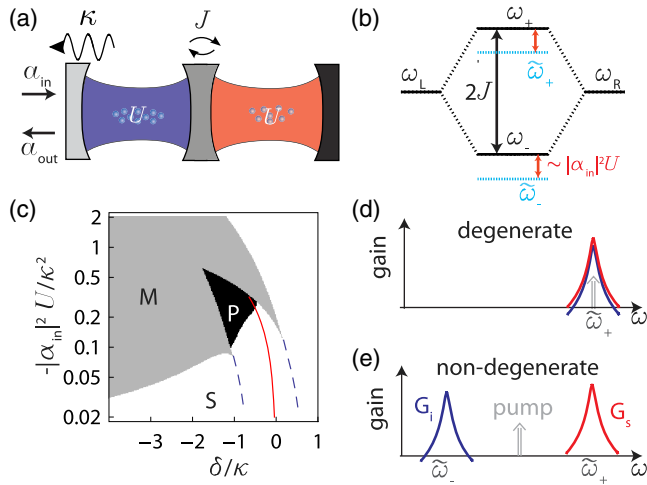
FIG. 1 (color online). (a) Optical frequency representation of the Bose-Hubbard dimer, illustrated as two cavities each with on-site interaction strength U and coupled with hopping rate J. The left cavity emits into a transmission line at rate κ. (b) Mode structure of the dimer and drive induced redshifts. See text for details. (c) Calculated phase diagram of the dimer driven with a coherent input field $\alpha_{\rm in}$ at detuning δ from the bare resonance frequency ω_0 for $J = 0.7\kappa$ and $U < 0$. The red line indicates drive configurations with a vanishing field amplitude in the left cavity. The dashed blue lines indicate redshifted frequencies, $\tilde{\omega}_-$ and $\tilde{\omega}_+$. (d) Driving the system at frequency $\tilde{\omega}_+$ (gray vertical arrow) results in degenerate parametric amplification, with signal gain G_s (red) and idler gain G_i (blue) both occupying the symmetric mode. (e) Signal and idler gain become nondegenerate when driving the system in between $\tilde{\omega}_+$ and $\tilde{\omega}_-$.

multiple classical solutions (M) or a region with a unique but parametrically unstable solution (P); see Fig. 1(c), Ref. [29], and the Supplemental Material [30]. When driving the dimer close to either one of the two redshifted eigenfrequencies $\tilde{\omega}_-$ or $\tilde{\omega}_+$, indicated by the blue dashed lines in Fig. 1(c), the system behaves like a single nonlinear cavity leaving the undriven mode idle. Close to the phase transition into the multistable region (M), the finite on-site interaction strength U stimulates the generation of signal-idler photon pairs. Since both signal and idler fields occupy the same mode, this is a degenerate parametric amplification process [15]; see the schematic representation in Fig. 1(d). However, when driving the dimer in between the two eigenfrequencies $\tilde{\omega}_-$ and $\tilde{\omega}_+$ [red line in Fig. 1(b)], resulting in an equal population of the symmetric and antisymmetric mode, we observe a fundamentally different behavior. In this case we approach the transition from the stable (S) into the para-metrically instable region (P), near which quantum fluctua-tions stimulate the generation of entangled photon pairs into the symmetric and antisymmetric mode at a rate diverging at the phase transition. When additional signal fields are applied to the dimer, nondegenerate amplification is expected at a large detuning on the order of $2J$ between signal and idler modes [Fig. 1(e)].

We demonstrate the phenomena discussed above in a circuit QED implementation of the Bose-Hubbard dimer which we chose to refer to as a Josephson parametric dimer (JPD). In the JPD, two interdigitated finger capacitors C_L and C_R shunted by an array of superconducting quantum interference devices (SQUIDs) form two lumped element oscillators in which the SQUIDs act as inductors [Fig. 2(a)]. The SQUID inductance, and with that the resonance frequencies of the JPD circuit, is tuned by applying an external magnetic field through a coil mounted on the sample holder. The SQUID nonlinearity leads to effective photon-photon interactions with a strength $U/2\pi \approx -E_c/hM^2 \approx -80$ kHz, which depends on the
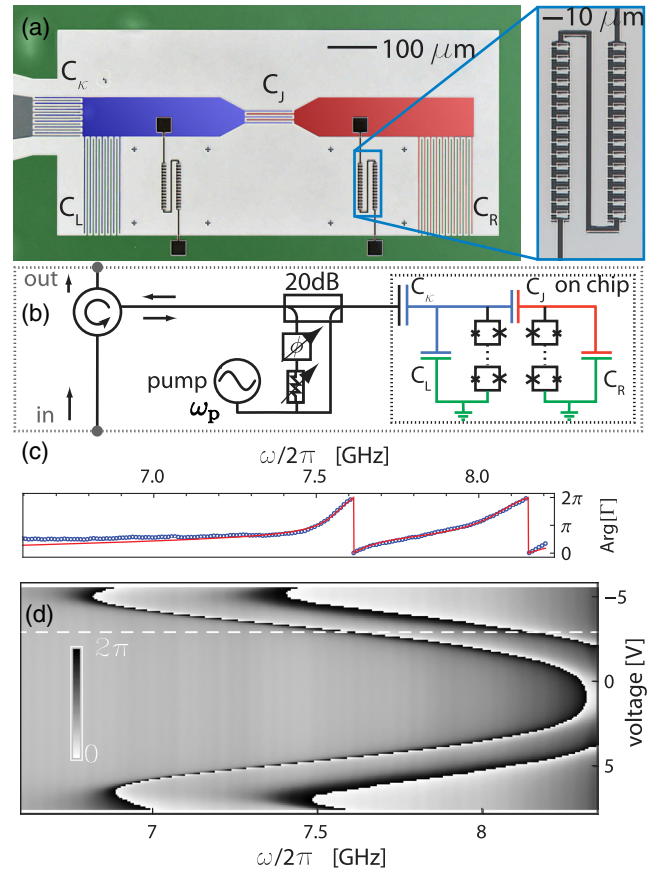
FIG. 2 (color online). (a) False-color micrograph of the sample. The interdigitated finger structures form the capacitors of two coupled oscillators. An effective nonlinear inductance is realized as an array of SQUIDs in each resonator, also shown enlarged. (b) Simplified circuit diagram of the experimental setup. The circuit is driven with a pump field at frequency $\omega_p = \omega_0 + \delta$ through a -20 dB directional coupler, of which the second port is used to interferometrically suppress the pump field reflected from the sample by more than -60 dB. Input and output signal fields are separated using a circulator. (c) Argument $\text{Arg}[\Gamma]$ of the measured (blue dots) and fitted (red line) reflection coefficient Γ vs probe frequency. (d) Measured $\text{Arg}[\Gamma]$ vs external magnetic flux which is controlled by a voltage applied to a coil biasing filter. The white dashed line indicates the data trace shown in (c).

charging energy $E_c \approx e^2/2C_R$ and can be controlled by varying the number of SQUIDs M in the array [31]. We set a lower bound to the critical current of each SQUID by using junctions with a ratio of Josephson energies given by $E_{J,1}/E_{J,2} \approx 1/3$. This choice avoids an uncontrolled increase in nonlinearity due to inhomogeneous coupling of SQUIDs to the external magnetic field; see the Supplemental Material for details [30]. The coupling rate between the two resonators $J \approx C_J \omega_0/4C_R$ is proportional to the capacitance C_J. C_κ determines the coupling κ to the input and output line. A circuit diagram of the JPD device illustrating its operation as an amplifier is shown in Fig. 2(b).

We have measured the argument of the reflection coefficient Arg[Γ] of the JPD in linear response using a weak test tone of frequency $\omega/2\pi$. As expected, we find two resonances, each leading to a phase shift of 2π in the reflected signal [Fig. 2(c)]. By fitting the data to the model obtained from input-output theory (Supplemental Material [30]), we extract the parameters $(\omega_L, \omega_R, \kappa, J)/2\pi \approx (7.8, 7.9, 0.32, 0.25)$ GHz for the bias point indicated by the dashed white line in Fig. 2(d). By varying the external magnetic field through the SQUID arrays, we tune both modes simultaneously [Fig. 2(d)]. As desired, the left and right modes are found to be sufficiently close to resonance $|\omega_L - \omega_R| \lesssim J, \kappa$ over the entire tuning range.

To achieve degenerate amplification, we drive the JPD with a coherent pump tone at frequency $\omega_p/2\pi = 7.98$ GHz close to the resonance frequency of the symmetric mode $\tilde{\omega}_+$. As expected, the measured signal and idler gains (red and blue points) are to very good approximation described by Lorentzian lines (black solid lines) for the two indicated pump powers [Fig. 3(a)].

While the degenerate amplification process is the conventional one in Josephson parametric amplifiers [15], we observe nondegenerate parametric amplification when driving the JPD in between the symmetric and antisymmetric mode. In this case the symmetric and antisymmetric modes of the JPD serve as signal and idler modes [Figs. 3(b) and 3(c)]. When amplifying a signal at $\omega_s/2\pi = 7.79$ GHz [Fig. 3(c)], the idler field is far detuned from

the signal field at $\omega_i/2\pi = (2\omega_p - \omega_s)/2\pi = 7.41$ GHz [Fig. 3(b)] allowing for simple rejection from the detection band for typical bandwidths of less than J as required for phase preserving amplification. The splitting between signal and idler gain maxima depends on both the pump power and the pump frequency. Individual adjustment of these parameters can therefore be used to independently fine-tune the maximum gain and the peak position while keeping the external magnetic flux constant. For the chosen drive parameters, the gain curves are well described by Lorentzian lines (black lines). In contrast to other implementations of nondegenerate parametric amplifiers [19], the JPD emits the signal and the idler fields into the same transmission line, which can therefore both be used for amplification. Furthermore, the compact lumped element design with its large participation ratio, and the use of SQUID arrays improve the achievable bandwidth and dynamic range [31] compared to existing nondegenerate amplifiers and provide a wide tunability.

For the measurements shown in Fig. 3(c) we have controlled the gain by varying the pump power. The fact that we can reach gain values of more than 50 dB (not shown) indicates that the amplifier is far from saturation when operated at moderate gain. In fact, for samples with larger $\kappa/|U|$, we have measured amplification with remarkable dynamic range specified by a 1 dB compression point at input signals of -110 dBm (2000 photons per μs) at a gain of 20 dB, as well as gain-bandwidth products of more than 250 MHz in the nondegenerate mode of operation. Further improvements in the dynamic range are expected to be straightforward to realize by increasing the number of SQUIDs in the arrays, by using Josephson junctions with even larger Josephson energy [32] and by increasing κ. In addition we suggest that as an alternative to the designs presented in Refs. [21,23] parametric amplifiers with well-controllable broadband amplification could be realized by extending the presented design to multicavity arrays.

In our experiments we probe the quantum nature of the observed parametric conversion processes by leaving the JPD input in the vacuum state and observing the creation of entangled photon pairs. The two-mode squeezing spectrum
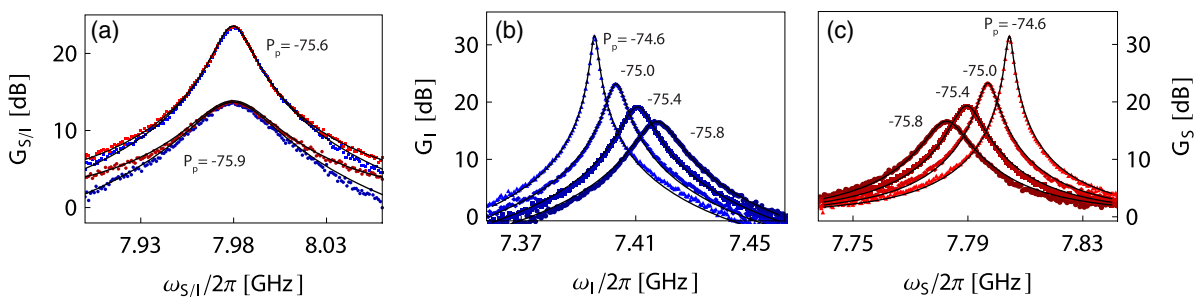
FIG. 3 (color online). (a) Measured signal (red) and idler gain (blue) vs frequency for two pump powers $P_p \approx \{-75.9, -75.6\}$ dBm fitted to a Lorentzian (black lines) for degenerate operation. (b),(c) Measured idler G_I and signal gain G_S for a nondegenerate operation together with Lorentzian fits (black lines) for drive powers $P_p \approx \{-75.8, -75.4, -75., -74.6\}$ dBm.

$S^{\phi}_{+-}(\Delta) \propto \mathrm{Var}[e^{-i\phi}a_{\Delta} + e^{i\phi}a^{\dagger}_{-\Delta}]$ (Supplemental Material [30]) is a direct measure of this Einstein-Podolsky-Rosen-type entanglement [33] and allows us to resolve the asymmetric frequency dependence of squeezing correlations. Here, a_{Δ} ($a_{-\Delta}$) is the annihilation operator for signal (idler) photons at detuning Δ ($-\Delta$) from the pump and ϕ is the phase of the pump relative to the local oscillator used for detection. Depending on the phase ϕ we observe noise squeezing (antisqueezing) below (above) the vacuum limit. The measured squeezing spectra, which are obtained after subtracting the calibrated detector noise, fit very well to our theoretical model (Supplemental Material [30]) and they accurately reproduce the spectral asymmetry for intermediate LO phases, as shown on a logarithmic scale relative to the vacuum level (0 dB) in Fig. 4(a). As a reference we also show the noise level when the JPD is turned off (gray points). The spectra also demonstrate that measured squeezing and antisqueezing are almost perfectly inversely proportional to each other. The value of the squeezing spectrum evaluated at the detuning indicated by the vertical dashed line in Fig. 4(a) shows the expected sinusoidal dependence on the phase ϕ; see the fit to theory (red line) in Fig. 4(b). The gain-dependent squeezing reaches values down to below -12 dB (see inset) in a bandwidth larger than 10 MHz which is, to the best of our knowledge, the largest value reported so far for

superconducting circuits [15,34–36]. We attribute deviations from the theoretically expected amount of squeezing at higher gain values to slow drifts of the pump relative to the local oscillator phase and slight depletion of the pump field at higher gain values.

To further investigate the statistical properties of the signal a_{+} and idler a_{-} fields and their correlations we have measured cumulants $\langle\langle(a^{\dagger}_{+})^{n}(a_{+})^{m}(a^{\dagger}_{-})^{k}(a_{-})^{l}\rangle\rangle$ with order (n, m, k, l) up to $n + m + k + l \leq 4$. The cumulant representation of correlators is particularly suitable to determine how well the analyzed radiation fields are described by ideal Gaussian states, since only the quadratic terms are expected to be nonzero. For this experiment we have used two detection channels to individually record the signal and idler radiation each in a 4 MHz band around their carrier frequencies [34,37]. We have extracted the cumulants based on histograms of the measured field quadratures (Supplemental Material [30]). While the (1,1,0,0) and the (0,0,1,1) terms describe the average quadrature fluctuations in the signal and idler fields, respectively, the large (0,1,0,1) term demonstrates the entanglement correlations between the two fields [Fig. 4(c)]. Except for the second order terms, all higher order cumulants vanish, as expected for an ideal Gaussian state. The Gaussian property is an essential requirement, when using this signal-idler entanglement as a resource in continuous variable quantum computation protocols [38]. This property is also highly relevant when employing the JPD for photon correlation measurements in which the statistical properties of the amplified field are to be preserved.

Our measurements highlight the excellent performance of the presented device and its potential to be broadly used in cryogenic setups aiming at quantum limited measurements—particularly in superconducting circuits. In addition to its practical use as an amplifier, the presented Bose-Hubbard dimer and its extension to larger arrays of cavities may prove interesting as an unconventional single photon source [39], for the study of Majorana modes in parametrically coupled cavities [40], and, in general, for experimental studies of nonequilibrium many-particle physics in photonic systems.

FIG. 4 (color online). (a) Two-mode squeezing spectrum $S^{\phi}_{+-}(\Delta)$ for local oscillator phases $\phi = \pi\{8,48,69,79,89\}/180$ with a global fit to the theoretical model. (b) Value of $S^{\phi}_{+-}(\Delta)$ at the sideband frequency $\Delta/2\pi = 157.5$ MHz indicated by the vertical dashed line in (a) vs local oscillator phase ϕ. The inset shows the value of squeezing at $\phi = \pi/2$ vs gain in comparison to the ideal theoretical value (red line). (c) Real and imaginary part of the measured cumulants $\langle\langle(a^{\dagger}_{+})^{n}(a_{+})^{m}(a^{\dagger}_{-})^{k}(a_{-})^{l}\rangle\rangle$ for indicated orders (n, m, k, l) up to $n + m + k + l \leq 4$.

*Present address: Department of Physics, Princeton University, Princeton NJ 08544, USA.
eichlerc@phys.ethz.ch

[1] A. A. Houck, H. E. Tureci, and J. Koch, Nat. Phys. **8**, 292 (2012).

[2] A. D. Greentree, C. Tahan, J. H. Cole, and L. C. L. Hollenberg, Nat. Phys. **2**, 856 (2006).

[3] D. G. Angelakis, M. F. Santos, and S. Bose, Phys. Rev. A **76**, 031805 (2007).

[4] M. J. Hartmann, F. G. S. L. Brandao, and M. B. Plenio, Nat. Phys. **2**, 849 (2006).

[5] D. Gerace, H. E. Tureci, A. İmamoğlu, V. Giovannetti, and R. Fazio, Nat. Phys. **5**, 281 (2009).

[6] M. Abbarchi, A. Amo, V. G. Sala, D. D. Solnyshkov, H. Flayac, L. Ferrier, I. Sagnes, E. Galopin, A. Lemaitre, G. Malpuech, and J. Bloch, Nat. Phys. **9**, 275 (2013).

[7] M. Ludwig, A. H. Safavi-Naeini, O. Painter, and F. Marquardt, Phys. Rev. Lett. **109**, 063601 (2012).

[8] T. A. Palomaki, J. W. Harlow, J. D. Teufel, R. W. Simmonds, and K. W. Lehnert, Nature (London) **495**, 210 (2013).

[9] H. Okamoto, A. Gourgout, C.-Y. Chang, K. Onomitsu, I. Mahboob, E. Y. Chang, and H. Yamaguchi, Nat. Phys. **9**, 480 (2013).

[10] H. S. J. van der Zant, F. C. Fritschy, W. J. Elion, L. J. Geerligs, and J. E. Mooij, Phys. Rev. Lett. **69**, 2971 (1992).

[11] S. Schmidt, D. Gerace, A. A. Houck, G. Blatter, and H. E. Türeci, Phys. Rev. B **82**, 100507 (2010).

[12] J. Raftery, D. Sadri, S. Schmidt, H. E. Türeci, and A. A. Houck, arXiv:1312.2963 [Phys. Rev. X (to be published)].

[13] C. M. Caves, Phys. Rev. D **26**, 1817 (1982).

[14] B. Yurke, P. G. Kaminsky, R. E. Miller, E. A. Whittaker, A. D. Smith, A. H. Silver, and R. W. Simon, Phys. Rev. Lett. **60**, 764 (1988).

[15] M. A. Castellanos-Beltran, K. D. Irwin, G. C. Hilton, L. R. Vale, and K. W. Lehnert, Nat. Phys. **4**, 929 (2008).

[16] E. Tholén, A. Ergül, E. Doherty, F. Weber, F. Grégis, and D. Haviland, Appl. Phys. Lett. **90**, 253509 (2007).

[17] T. Yamamoto, K. Inomata, M. Watanabe, K. Matsuba, T. Miyazaki, W. D. Oliver, Y. Nakamura, and J. S. Tsai, Appl. Phys. Lett. **93**, 042510 (2008).

[18] D. Kinion and J. Clarke, Appl. Phys. Lett. **92**, 172503 (2008).

[19] N. Bergeal, F. Schackert, M. Metcalfe, R. Vijay, V. E. Manucharyan, L. Frunzio, D. E. Prober, R. J. Schoelkopf, S. M. Girvin, and M. H. Devoret, Nature (London) **465**, 64 (2010).

[20] D. Hover, Y.-F. Chen, G. J. Ribeill, S. Zhu, S. Sendelbach, and R. McDermott, Appl. Phys. Lett. **100**, 063503 (2012).

[21] B. Ho Eom, P. K. Day, H. G. LeDuc, and J. Zmuidzinas, Nat. Phys. **8**, 623 (2012).

[22] B. Abdo, K. Sliwa, L. Frunzio, and M. Devoret, Phys. Rev. X **3**, 031001 (2013).

[23] J. Y. Mutus, T. C. White, R. Barends, Y. Chen, Z. Chen, B. Chiaro, A. Dunsworth, E. Jeffrey, J. Kelly, A. Megrant, C. Neill, P. J. J. O'Malley, P. Roushan, D. Sank, A. Vainsencher, J. Wenner, K. M. Sundqvist, A. N. Cleland, and J. M. Martinis, Appl. Phys. Lett. **104**, 263513 (2014).

[24] A. A. Clerk, M. H. Devoret, S. M. Girvin, F. Marquardt, and R. J. Schoelkopf, Rev. Mod. Phys. **82**, 1155 (2010).

[25] R. Vijay, D. H. Slichter, and I. Siddiqi, Phys. Rev. Lett. **106**, 110502 (2011).

[26] D. Ristè, C. C. Bultink, K. W. Lehnert, and L. DiCarlo, Phys. Rev. Lett. **109**, 240502 (2012).

[27] D. Sank, E. Jeffrey, J. Y. Mutus, T. C. White, J. Kelly, R. Barends, Y. Chen, Z. Chen, B. Chiaro, A. Dunsworth, A. Megrant, P. J. J. O'Malley, C. Neill, P. Roushan, A. Vainsencher, J. Wenner, A. N. Cleland, and J. M. Martinis, arXiv:1401.0257.

[28] C. Eichler, D. Bozyigit, and A. Wallraff, Phys. Rev. A **86**, 032106 (2012).

[29] D. Sarchi, I. Carusotto, M. Wouters, and V. Savona, Phys. Rev. B **77**, 125324 (2008).

[30] See the Supplemental Material at http://link.aps.org/supplemental/10.1103/PhysRevLett.113.110502 for details.

[31] C. Eichler and A. Wallraff, EPJ Quantum Technology **1**, 2 (2014).

[32] F. Lecocq, I. M. Pop, Z. Peng, I. Matei, T. Crozes, T. Fournier, C. Naud, W. Guichard, and O. Buisson, Nanotechnology **22**, 315302 (2011).

[33] A. Miranowicz, M. Bartkowiak, X. Wang, Y.-x. Liu, and F. Nori, Phys. Rev. A **82**, 013824 (2010).

[34] C. Eichler, D. Bozyigit, C. Lang, M. Baur, L. Steffen, J. M. Fink, S. Filipp, and A. Wallraff, Phys. Rev. Lett. **107**, 113601 (2011).

[35] E. Flurin, N. Roch, F. Mallet, M. H. Devoret, and B. Huard, Phys. Rev. Lett. **109**, 183901 (2012).

[36] E. P. Menzel, R. Di Candia, F. Deppe, P. Eder, L. Zhong, M. Ihmig, M. Haeberlein, A. Baust, E. Hoffmann, D. Ballester, K. Inomata, T. Yamamoto, Y. Nakamura, E. Solano, A. Marx, and R. Gross, Phys. Rev. Lett. **109**, 250502 (2012).

[37] C. Lang, C. Eichler, L. Steffen, J. M. Fink, M. J. Woolley, A. Blais, and A. Wallraff, Nat. Phys. **9**, 345 (2013).

[38] S. L. Braunstein and P. van Loock, Rev. Mod. Phys. **77**, 513 (2005).

[39] T. C. H. Liew and V. Savona, Phys. Rev. Lett. **104**, 183601 (2010).

[40] C.-E. Bardyn and A. İmamoğlu, Phys. Rev. Lett. **109**, 253606 (2012).